Analysis and Design of Sub-Harmonically Injection Locked Oscillators

Arkosnato Neogy and Jaijeet Roychowdhury
Department of Electrical Engineering and Computer Sciences, University of California at Berkeley

Abstract— **Sub-harmonic injection locking (SHIL) is an interesting phenomenon in nonlinear oscillators that is useful in RF applications, *e.g.*, for frequency division. Existing techniques for analysis and design of SHIL are limited to a few specific circuit topologies. We present a general technique for analysing SHIL that applies uniformly to any kind of oscillator, is highly predictive, and offers novel insights into fundamental properties of SHIL that are useful for design. We demonstrate the power of the technique by applying it to ring and LC oscillators and predicting the presence or absence of SHIL, the number of distinct locks and their stability properties, lock range, *etc.*. We present comparisons with SPICE-level simulations to validate our method's predictions.**

I. INTRODUCTION

Injection locking (IL) [1], [2], [3] is a nonlinear phenomenon in which a self-sustaining oscillator's phase becomes precisely locked (*i.e.*, entrained or synchronized) to that of an externally applied signal. The phenomenon, together with the related effect of injection pulling, has often been regarded as an unwanted disturbance, causing, among other things, malfunction in serial clock/data recovery, increased timing jitter and clock skew, increased BER in communications, *etc.*. Over the years, however, IL has also been put to good use in electronics – *e.g.*, for quadrature signal generation [4]; for microwave generators in laser optics [5]; for fast, low-power frequency dividers [6]; and in PLLs [7] and wireless sensor networks [8]. Moreover, IL is an important enabling mechanism in biology (*e.g.*, [9], [10]).

When an oscillator locks to an external signal whose frequency is close to the oscillator's natural frequency, the phenomenon is termed *fundamental harmonic IL*. It is also possible, however, for oscillators to phase-lock at a frequency that is an *exact integral sub-multiple* of the frequency of the externally applied signal; this is termed *sub-harmonic IL* (or SHIL, described further in Sec. II-B) and is useful in frequency division applications [6], [7].

Design of circuits exploiting SHIL has tended to rely predominantly on trial-and-error based methodologies, using brute-force transient simulations to assess impact on SHIL-based circuit function. Existing analyses of fundamental and sub-harmonic IL (*e.g.*, [11], [2], [12]) have been limited to very specific circuit topologies (*e.g.*, LC oscillators), while more general analyses [13], that apply to any kind of oscillator, do not consider SHIL. The work of Daryoush *et. al.* [14] presented a computationally complicated method limited to negative feedback oscillators, and provided no insights about multiple lock states for SHIL. To our knowledge, there is no general analysis or theory that provides the correct design intuition and predictive power for SHIL and related phenomena.

In this paper, we develop and validate a general method for analysing and understanding sub-harmonic injection locking. The method applies to any self-sustaining, amplitude-stable oscillator, not only from electronics but also from other domains such as biology. Specifically, we obtain a simple equation that not only has numerical uses for fast simulation of sub-harmonic injection pulling and locking, but can be depicted graphically, thereby offering powerful insights into qualitative and quantitative properties of SHIL in oscillators. One important such insight is that m^{th}-sub-harmonic locking is intimately related to the mth-harmonic component of the PPV function [15], [16], [17] (see Sec. II-A); our analysis provides quantitative design guidelines for inducing m^{th}-sub-harmonic locking. Another important insight is that m^{th}-sub-harmonic locking typically occurs in one of $2m$ distinct phases (relative to a reference signal at the same frequency);

m of these solutions, spaced uniformly in phase increments of $\frac{2\pi}{m}$, are dynamically stable.

Development of our method starts from a scalar, non-linear equation (the PPV equation [15], [16], [17], described further in Sec. II-A) that governs the phase dynamics of oscillators. We devise a specialized analysis of the PPV equation by first recasting it in terms of a phase error metric that detects SHIL, then averaging out fast variations[1] to obtain a simple scalar differential equation in the phase error metric. "DC" analysis of this equation captures SHIL and provides the insights noted above. A key quantity needed in these equations, the PPV function specific to a given oscillator, is obtained via efficient and robust numerical methods [17].

We present extensive numerical experiments that compare detailed SPICE-level simulations with our new SHIL analysis and validate its accuracy and predictive nature. Using ring and LC oscillators as examples, we apply our technique to determine whether or not SHIL can occur in a given design, in how many distinct ways lock can occur, how robust a lock is, how an existing design can be modified to better induce SHIL, *etc.*. We also prove the existence of multiple distinct locks using detailed SPICE-level simulations.

The remainder of the paper is organized as follows. Sec. II provides brief background on PPV phase equations and basic concepts of sub-harmonic IL. Sec. III-A presents our new analysis of SHIL, while Sec. III-B discusses key uses and insights that stem from this analysis. Sec. IV presents numerical experiments on ring and LC oscillators that validate our approach.

II. PRELIMINARIES

A. The PPV Nonlinear Phase Equation for Oscillators

A SPICE-level representation of any circuit (including oscillators) is equivalent [18] to a system of differential-algebraic equations (DAEs) [19] in the form:

$$\frac{d}{dt}\vec{q}(\vec{x}(t)) + \vec{f}(\vec{x}) + \vec{b}(t) = \vec{0}, \qquad (1)$$

where $\vec{x}$ denotes internal state, $\vec{f}(\cdot)$ and $\vec{q}(\cdot)$ capture static and dynamic terms, respectively, and $\vec{b}(t)$ denotes inputs to the system. Self-sustaining autonomous oscillators, by their nature, produce periodic, time-varying solutions $\vec{x}(t)$ even when $\vec{b}(t)$ vanishes (or is constant with time) — this is termed natural oscillation. Denote such natural oscillation by $\vec{x}_s(t)$ and its period by T. For a large class of self-sustaining oscillators, it has been shown [16] that if natural oscillation is disturbed by *small* time-varying external inputs $\vec{b}(t)$, the oscillator's response can be approximated well as

$$\vec{x}(t) \simeq \vec{x}_s(t + \alpha(t)), \qquad (2)$$

where $\alpha(t)$, a time shift caused by the external inputs, is governed by the scalar differential equation

$$\frac{d}{dt}\alpha(t) = \vec{v}_1^T(t + \alpha(t)) \cdot \vec{b}(t). \qquad (3)$$

In (3), the vector $\vec{v}_1(t)$, known as the Phase Response Curve (PRC) [15] or Perturbation Projection Vector (PPV) [17], is a T-periodic

---

[1]in a manner similar to that used to derive Adler's equation for fundamental harmonic IL [1], [13].

vector function of time. For the purposes of this paper, we rewrite (3) by defining a 1-periodic version of the PPV, *i.e.*,

$$\vec{p}(t) = \vec{v}_1(Tt), \tag{4}$$

and using this in (3) to obtain

$$\frac{d}{dt}\alpha(t) = \vec{p}^T(ft + f\alpha(t)) \cdot \vec{b}(t), \tag{5}$$

where $f \triangleq \frac{1}{T}$. (5), known as the PPV equation or the PPV phase macromodel, is the starting point for our SHIL analysis in Sec. III-A.

B. Basic Concepts of Sub-harmonic Phase Locking

Given any T periodic function $s(t)$, if another function $r(t)$ is derived from it as $r(t) \triangleq s(\phi(t))$, then $\phi(t)$ is termed the *phase* of $r(t)$ with respect to the base period T^2. For example, if $s(t)$ is the 1-periodic sinusoid $s(t) = \sin(2\pi t)$ and

$$\text{REF}(t) \triangleq s(f_0 t), \tag{6}$$

then the phase of $\text{REF}(t)$ with respect to the base period 1 is

$$\phi_{\text{REF}}(t) \triangleq f_0 t. \tag{7}$$

Suppose we are given another signal $y(t)$ with phase $\phi_y(t)$ (with respect to the same base period as $\text{REF}(t)$). Then $\text{REF}(t)$ is said to in "simple m^{th} sub-harmonic phase lock" to $y(t)$ if

$$\phi_{\text{REF}}(t) = \frac{\phi_y(t)}{m} + \text{const.} \tag{8}$$

For example, if $y(t) \triangleq \cos(2\pi \cdot 3 \cdot f_0 t + 0.5)$, then $\phi_{\text{REF}}(t)$ in (6) is in simple 3rd sub-harmonic phase lock to $y(t)$.

We now establish terminology that will be used in the remainder of the paper. The natural period of any oscillator will be denoted by T; its natural frequency, $\frac{1}{T}$, will be denoted by f. External inputs to the oscillator will be denoted by $\overrightarrow{\text{SYNC}}(t)$, with frequency f_{in} and phase $\phi_{in}(t) = f_{in}t$; *i.e.*, $\vec{b}(t)$ in (1) is given by

$$\vec{b}(t) = \overrightarrow{\text{SYNC}}(t) = \vec{c}(\phi_{in}(t)), \tag{9}$$

where $\vec{c}(t) \triangleq \vec{b}(\frac{t}{f_{in}})$ is 1-periodic.

If $\vec{b}(t) = \overrightarrow{\text{SYNC}}(t)$ results in m^{th} sub-harmonic lock, then $f_{in} \sim mf$; define Δf by $f_{in} = m(f + \Delta f)$. Denote the frequency of mth sub-harmonic lock to $\overrightarrow{\text{SYNC}}(t)$ by f_0; *i.e.*, $f_0 = \frac{f_{in}}{m} = f + \Delta f$. Finally, denote $\text{REF}(t)$ to be a reference signal, at frequency f_0, that is in m^{th} sub-harmonic phase lock to the external input signal $\overrightarrow{\text{SYNC}}(t)$.

III. ANALYSING THE PPV EQUATION TO CAPTURE SHIL

A. Derivation of the Alderized SHIL equation

We now proceed to analyse SHIL by expressing the PPV equation (5) equation in terms of phase. We assume that the external input $\vec{b}(t)$ equals the $\overrightarrow{\text{SYNC}}(t)$ signal defined in Sec. II-B, with frequency $f_{in} = mf_0$ and phase $\phi_{in}(t) = f_{in}t$.

From (2), observe that the phase of the oscillator's response under external perturbation is $\phi(t) \triangleq ft + f\alpha(t)$. Rewriting the PPV equation (5) in terms of $\phi(t)$, we obtain

$$\frac{d}{dt}\phi(t) = f + f\vec{p}^T(\phi(t)) \cdot \vec{c}(\phi_{in}(t)). \tag{10}$$

Define the mth-*SHIL phase error* to be

$$\theta(t) \triangleq \phi(t) - \frac{1}{m}\phi_{in}(t). \tag{11}$$

This definition is motivated by the fact that if the oscillator achieves simple m^{th} sub-harmonic phase lock to its external input $\overrightarrow{\text{SYNC}}(t)$,

then $\theta(t) \equiv$ constant. Taking the time-derivative of (11) and using (10) and the definition of $\phi_{in}(t)$ from Sec. II-B, we obtain

$$\dot{\theta}(t) = (f - \frac{1}{m}f_{in}) + f\left(\vec{p}^T(\theta(t) + \frac{1}{m}f_{in}t) \cdot \vec{c}(f_{in}t)\right). \tag{12}$$

Now, $\vec{p}(\cdot)$ is a 1-periodic function, hence $\vec{p}(\theta(t) + \frac{1}{m}f_{in}t)$ may be expressed using Fourier series as

$$\vec{p}\left(\theta(t) + \frac{1}{m}f_{in}t\right) = \sum_{k=-\infty}^{\infty} \vec{p}_k e^{j2\pi k(\theta(t) + \frac{1}{m}f_{in}t)}, \tag{13}$$

where $\{\vec{p}_k\}$ are the Fourier coefficients[3] of $\vec{p}(t)$. Similarly, $\vec{c}(t)$ being a 1-periodic function, we have

$$\vec{c}(f_{in}t) = \sum_{l=-\infty}^{\infty} \vec{c}_l e^{j2\pi l f_{in}t}, \tag{14}$$

with $\{\vec{c}_k\}$ being the Fourier coefficients of $\vec{c}(t)$. Using (13) and (14) in (12), we arrive at

$$\dot{\theta}(t) = \left(f - \frac{1}{m}f_{in}\right) + f\sum_{k,l=-\infty}^{\infty} \vec{p}_k \cdot \vec{c}_l e^{j2\pi(f_{in}t(l+\frac{k}{m})+k\theta(t))}. \tag{15}$$

The double summation term in (15) contains fast-varying components (stemming from non-zero coefficients of $f_{in}t$ in the exponential), together with potentially slowly varying components resulting from the $k\theta(t)$ terms. This equation can be simplified under the assumptions that 1) $\theta(t)$ is slowly-varying with respect to time-scales of the order of $\frac{m}{f_{in}}$, and 2) $\vec{p}^T(\cdot)$ is smooth, *i.e.*, it does not feature large changes over any argument interval of length $\ll 1$. Defining $T_{in} = \frac{1}{f_{in}}$ and

$$\theta_a(t) \triangleq \frac{1}{mT_{in}}\int_{t-\frac{mT_{in}}{2}}^{t+\frac{mT_{in}}{2}} \theta(\tau)\,d\tau, \tag{16}$$

it is easily shown under the above assumptions that

$$\dot{\theta}_a(t) = \left(f - \frac{1}{m}f_{in}\right) + f\sum_{l=-\infty}^{\infty} \vec{p}_{-ml} \cdot \vec{c}_l e^{-j2\pi ml\theta_a(t)}. \tag{17}$$

If the oscillator achieves simple m^{th} sub-harmonic phase lock, then, as noted earlier, $\theta(t) \equiv \theta_a(t) \equiv$ constant, *i.e.*, $\dot{\theta}(t) \equiv 0$; hence (17) reduces to

$$\boxed{\frac{f_{in}-mf}{mf} = g(\theta) \triangleq \sum_{l=-\infty}^{\infty} \vec{p}_{-ml} \cdot \vec{c}_l e^{-j2\pi ml\theta}.} \tag{18}$$

(18), dubbed the *Adlerized[4] SHIL equation*, is a simple scalar algebraic equation in the SHIL phase error θ, solutions to which determine whether or not m^{th} sub-harmonic phase lock is possible. Observe that the LHS of (18) is a constant equalling $\frac{\Delta f}{f}$, while its RHS $g(\theta)$ is a real periodic function with period $\frac{1}{m}$. (18) can easily be plotted graphically; for example, as in Fig. 2(d) and Fig. 5(d), discussed further in Sec. IV. The significance of (18), and the insights it provides into SHIL, are discussed in the next section.

B. Insights resulting from the Adlerized SHIL equation

The simplicity of the form of equation (18) allows several interesting and useful design insights to be deduced from it. Typically, circuit designers are interested in design variables such as injection amplitude, lock range, stability of lock, *etc.*, regarding which (18) provides useful qualitative and quantitative information. (18) also provides additional insights into the very mechanisms of lock, which translate into key guidelines for designing oscillators for SHIL.

1) *Number, stability and spacing of distinct sub-harmonic locks*:
   From the facts that the RHS of (18), $g(\theta)$, is continuous,

---

[2]For convenience, we will omit "with respect to ..." when the base period is implicitly understood (*e.g.*, it is usually 1 in this paper).

[3]Given the differential equations (1) of any oscillator, robust and scalable numerical methods for finding $\{\vec{p}_k\}$ are available and well established [17].

[4]The form of (18) is similar to the well-known Adler equation [1] for fundamental-harmonic injection locking in negative resistance LC oscillators.

bounded, differentiable and $\frac{1}{m}$-periodic, it can be easily proved[5] that the number of distinct solutions of (18) is an integral multiple of $2m$ – *i.e.*, (18) can have zero, $2m$, $4m$, *etc.* solutions in interval $\theta \in [0,1)$. There will be no solutions if the value of the LHS of (18) falls outside the range of $g(\theta)$; this indicates that m^{th} sub-harmonic phase lock is not possible – as depicted in Fig. 9(b), discussed in Sec. IV. When the LHS does fall within the range of $g(\theta)$, $2m \times k$ solutions can exist – the typical case being $k = 1$ or $2m$ solutions, depicted in Fig. 2(d) and Fig. 5(d). Moreover, it can be shown that exactly half the solutions are dynamically stable, with the other half being unstable; indeed, stable and unstable solutions occur alternately. The separation between successive stable solutions (and between successive unstable solutions) is always $\frac{1}{m}$; however, the gaps in phase between a stable solution and its two neighbouring unstable solutions can be (and typically are) asymmetric. Fig. 2(d) and Fig. 5(d) illustrate these facts.

The fact that there are multiple stable solutions spaced at phase differences of $\frac{1}{m}$ increases the possibility that disturbances will lead to small phase slips when $m > 1$, compared to fundamental IL situations where $m = 1$, potentially leading to increased jitter concerns during design. Moreover, because of the asymmetric spacing of neighbouring unstable solutions, the magnitude of the phase disturbance needed to induce a phase slip depends on whether its sign is positive or negative. To assess lock robustness, the lesser of the gaps from a stable lock to its neighbouring unstable locks should considered during design.

2) *The mth harmonic of the PPV enables m^{th} sub-harmonic lock*:
From the definition (18) of $g(\theta)$, observe that the coefficient of the lth harmonic component of $g(\theta)$ is $\vec{p}_{-ml} \cdot \vec{c}_l$. This shows that the strength of the mth harmonic component of the PPV is of key importance in enabling m^{th} harmonic SHIL. For example, if the second harmonic component of the PPV is much smaller than its first and third harmonic components (as in Fig. 7(c), for the symmetric ring oscillator example of Sec. IV-B), then the oscillator is much more susceptible to first- and third-sub-harmonic IL than to second-sub-harmonic IL, for external inputs of the same magnitude. To make it better suited for second sub-harmonic locking (for example), the oscillator's design needs to be changed such that its PPV's second harmonic component is accentuated. This can be achieved, for example, by resizing the transistors in the oscillator's inverters to make them asymmetric as in Sec. IV-A1, resulting in the new PPV harmonics shown in Fig. 2(c). Note also that the presence of higher harmonics in the input, together with corresponding harmonics in the oscillator's PPV, facilitate m^{th} sub-harmonic lock – indicating that nonlinearity is useful for SHIL. Thus, the Adlerized SHIL equation (18), together with computational tools for determining the PPV's harmonics [17], provides concrete design guidelines for utilizing SHIL.

3) *Analytical lock range formulæ for sinusoidal inputs*: When the injected signal is purely sinusoidal (*i.e.*, $\vec{c}_k \equiv \vec{0}, \forall k \neq \pm 1$), as it can be in applications, $g(\theta)$ becomes purely sinusoidal too, enabling simple analytical formulæ to be derived that express the SHIL lock range $\frac{\Delta f}{f}$ in terms of injection amplitude, and vice-versa[6]. The relationship stands as

$$\frac{f_{in} - mf}{mf} = \frac{1}{2} \cdot P_m \cdot C \cdot \cos\left(2\pi m\theta\right) \quad (19)$$

where P_m denotes the real magnitude of the mth harmonic component of the PPV and C denotes the amplitude of the purely sinusiodal injected signal. (19) is derived by simplifying the RHS of (18) using $l = \pm 1$ only.

[5]The proof is omitted in the interest of brevity.
[6]Similar to formulæ for fundamental harmonic IL [20].

IV. VALIDATION ON RING AND LC OSCILLATORS

In this section, the theoretical predictions and insights of (18) developed in Sec. III-A and Sec. III-B are validated against full SPICE-level transient simulations, in the presence of the external injected signal $\overrightarrow{\text{SYNC}}(t)$. For the sake of brevity, the validation is performed on two circuits - a 3-stage CMOS
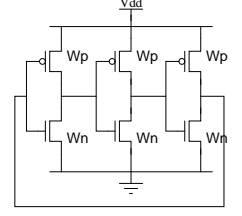

Fig. 1: 3-stage ring oscillator.

inverter based ring oscillator and an LC oscillator with a tanh negative-resistance nonlinearity. The experiments are performed on both the circuits for 2nd sub-harmonic injection locking, and on the ring oscillator only for 3rd sub-harmonic injection locking, but with additional modifications to the injection amplitude and locking range under 3 representative cases. The general flow of the experiments is as follows. First, the natural transient of the oscillator is observed and the resulting PPV waveforms plotted in the time and frequency domains, with necessary modifications to the oscillator to induce SHIL. Then, the design formula (18) is plotted graphically to explore the nature and possibility of SHIL. Finally, a full transient simulation of the oscillator in the presence of the external $\overrightarrow{\text{SYNC}}(t)$ injection is performed; the output waveforms are compared against the reference signal REF(t). It is important to emphasize that insights from plots of (18) are only qualitative and not strictly quantitative, since they are subject to the slowly-varying approximation for $\theta(t)$ noted Sec. III-A. In contrast, full transient analysis (which does not use (18) in any way) is precise. Thus, it should not be expected that the predicted phase for a successful lock in Fig. 2(d) will match exactly with the actual one in Fig. 3. However, it is reasonable to expect them to be close; indeed, certain qualitative features (*e.g.*, that the difference between the phases for two lock states should be π precisely) may be identical. Predictions from the design formula and observations from numerical experiments are thus cross-checked and validated.

A. 2nd Sub-Harmonic Injection Locking with 2 stable locks

We first apply the Adlerized SHIL equation (18) to explore 2nd sub-harmonic IL in two different types of oscillators, the 3-stage CMOS-based ring oscillator in Fig. 1 and the negative-resistance
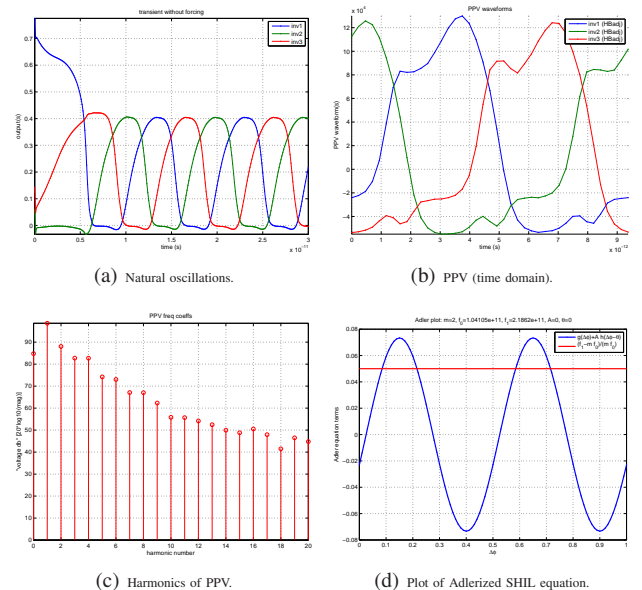

(a) Natural oscillations.

(b) PPV (time domain).

(c) Harmonics of PPV.

(d) Plot of Adlerized SHIL equation.

Fig. 2: Asymmetrized ring oscillator: natural oscillations, PPV waveforms and Adlerized SHIL plot.
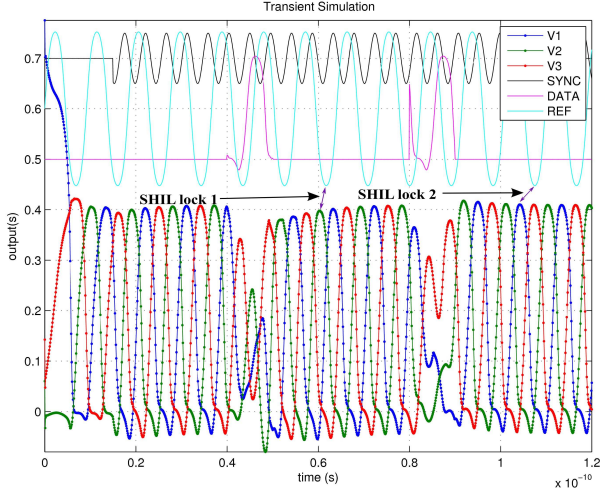
Fig. 3: Asymmetrized ring osc. transient simulation, showing two distinct SHIL lock states.

LC oscillator in Fig. 4. We also validate the predictions of (18) against detailed SPICE-level transient simulations. The external input $(\overrightarrow{\text{SYNC}}(t)$, defined in Sec. II-B) was applied as three current injections to the inverter nodes of the ring oscillator; for the LC oscillator, a single current injection was applied to the LC tank.

1) Asymmetric Ring Oscillator, $m = 2$ Sub-Harmonic Lock: As noted in Sec. III-B, item 2, the 2nd harmonic of the PPV is crucial to an oscillator's susceptibility to 2nd sub-harmonic lock. If the transistors in each inverter in Fig. 1 are sized symmetrically, the waveforms of natural oscillation become symmetric (about a DC value of approximately half its amplitude). This results in considerable suppression of even harmonics, in both the natural oscillation waveform and the oscillator's PPV waveforms (as depicted in Fig. 7(c)) — thereby making symmetric ring oscillators unsuitable for $m = 2$ SHIL.

However, it is easy to modify the inverter design to generate a strong 2nd harmonic PPV component. Asymmetrizing the sizes of the P and N transistors makes the natural oscillation waveform asymmetric about its mean, thus generating second harmonic components. In our design, we chose $W_P = 2\mu$m and $W_N = 0.3\mu$m to asymmetrize the oscillator; the resulting natural oscillation waveform and PPV harmonics are shown in Fig. 2(a) and Fig. 2(c), respectively. Time-domain waveforms of the PPV are also shown, in Fig. 2(b).

Fig. 2(d) depicts the LHS (red constant line) and RHS (blue sinusoidal waveform) of the Adlerized SHIL equation (18); intersections represent solutions. Observe that (as noted in Sec. III-B, item 2) there are 4 intersections, *i.e.*, 4 solutions. It can be shown that the second and fourth solutions (from the left), corresponding to negative slopes of the RHS waveform $g(\theta)$, are stable; the first and third solutions, where the slope of $g(\theta)$ is positive, are unstable. The two stable solutions are separated by $\Delta\theta = \frac{1}{2}$; similarly for the unstable solutions.

To validate the predictions of lock in Fig. 2(d), detailed SPICE-level transient simulations of ring oscillator were carried out; the results are shown in Fig. 3. The voltage waveforms of the sub-harmonically locked ring oscillator at the three inverter nodes are depicted in red, blue and green, respectively; the external input $\overrightarrow{\text{SYNC}}(t)$ is depicted in black; and the REF(t) signal by the sinusoidal waveform in turquoise. As indicated in the figure by "SHIL lock 1" and "SHIL lock 2", there are two distinct phase relationships between REF(t) and the oscillator's waveforms; close inspection shows that they are shifted by exactly half of an oscillation cycle. Indeed, as also shown in the figure, momentary disturbances (indicated by the magenta waveform) shift the oscillator's waveforms from one lock state to the other.
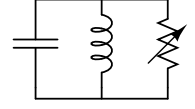
2) LC Oscillator in Binary Locking: The natural oscillation waveforms of the LC oscillator in Fig. 4 are shown in Fig. 5(a). The waveform depicted in blue represents the natural oscillations of the voltage across the capacitor (V_{cap}) of

Fig. 4: LC oscillator with tanh nonlinearity.

Fig. 4 and the green waveform depicts the oscillations of the inductor current, the latter being of significantly less amplitude than the former.

The time and frequency domain plots of the PPV waveforms for the V_{cap} are shown in blue in Fig. 5(b) and Fig. 5(c), respectively. As explained previously, the magnitude of the 2nd harmonic in the PPV waveform suggests the suitability of this oscillator for $m = 2$ SHIL. Fig. 5(d) shows the Adlerized plot for (18) for the LC oscillator. As before, the LHS (red constant line) and RHS (blue sinusiodal waveform) are observed to intersect at 4 distinct points; thus there are 4 solutions of (18) for the given situation, of which the second and fourth solutions from the left occuring on the negative slope of the RHS waveform are stable and the other two are unstable, as explained previously. Fig. 6 shows the validation against SPICE-level transient simulation of the LC oscillator in presence of the injected signal $\overrightarrow{\text{SYNC}}(t)$, depicted in black; the output is observed against REF(t), depicted in turquoise. As before, two distinct phase relationships are visible between the blue V_{cap} oscillation waveform and REF(t), which denote the 2 stable solutions of (18) under phase-locked condition. Disturbances (depicted by the magenta waveform) shift the oscillator's response by $\Delta\theta = \frac{1}{2}$ from one stable solution to another.

B. $m = 3$ Sub-harmonic Injection Locking with 3 stable states

The agreement between the Adlerized SHIL equation (18) and full SPICE-level transient simulation is further tested for 3rd sub-harmonic injection locking. As explained previously in Sec. II-B, this means that the injected signal $\overrightarrow{\text{SYNC}}(t)$ runs at a frequency $f_{in} = 3(f + \Delta f)$, f being the natural frequency of the oscillator. The circuit used for the validation is a 3-stage ring oscillator; however, for $m = 3$ SHIL the magnitude of the 3rd PPV harmonic is of significance as opposed to the 2nd. Therefore, unlike the asymmetrized design of Sec. IV-A1, an accentuation of the 3rd harmonic of the PPV is

(a) Natural oscillations.

(b) PPV (time domain).

(c) Harmonics of capacitor voltage PPV component.
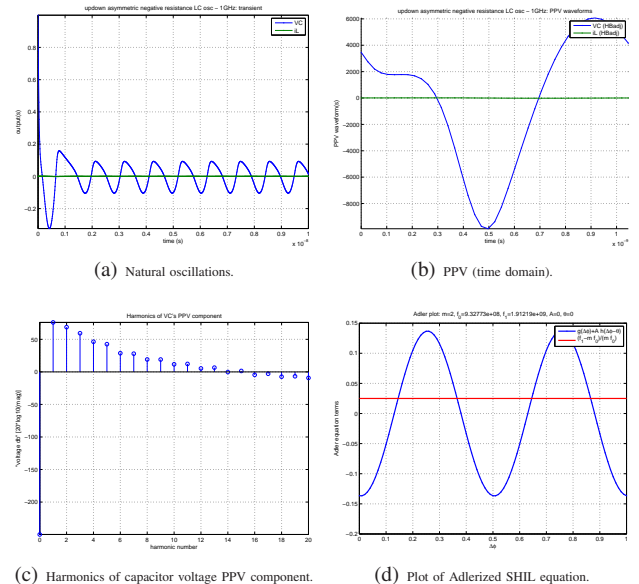

(d) Plot of Adlerized SHIL equation.

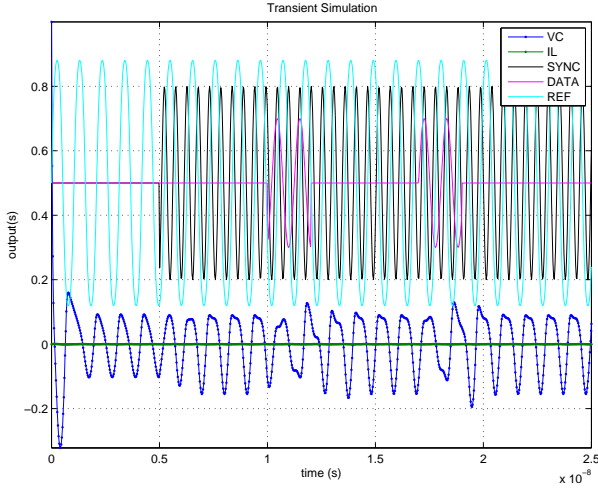Fig. 5: LC oscillator: natural oscillations, PPV waveforms and Adlerized SHIL plot.

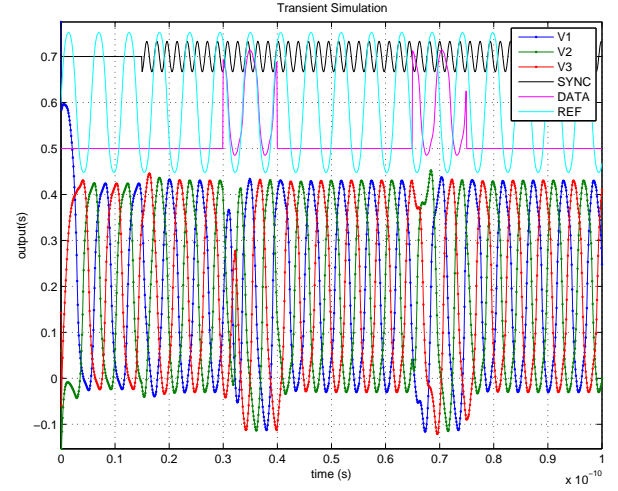Fig. 6: LC oscillator transient simulation, showing two distinct SHIL lock states.

Fig. 8: Symmetric ring oscillator transient simulation depicting robust SHIL in distinct lock states.
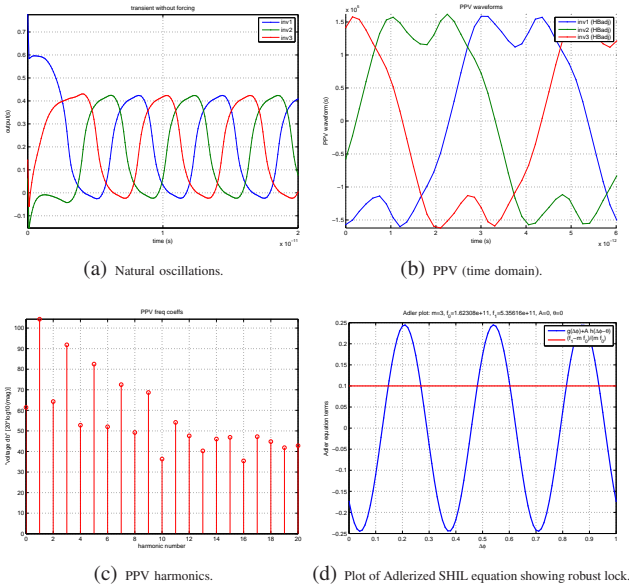

(a) Natural oscillations.

(b) PPV (time domain).

(c) PPV harmonics.

(d) Plot of Adlerized SHIL equation showing robust lock.

Fig. 7: Symmetric ring oscillator: natural oscillations, PPV waveforms and Adlerized SHIL plot.

The three cases are motivated by the observation that in the Adler/design formula plots, the red constant waveform representing the LHS of (18) essentially simplifies to the fractional frequency deviation $\left(\frac{\Delta f}{f}\right)$, while amplitude of the blue sinusiodal waveform, depicting the RHS of (18), reflects the injection amplitude of $\overrightarrow{SYNC}(t)$. Changing the frequency deviation or injection amplitude affects the magnitude of the red constant line (LHS) or the amplitude of the blue waveform (RHS), thus presenting an opportunity to critically examine the predictive power of (18).

Fig. 7(d) shows the Adler plot for case (a). The waveforms depicting the RHS and LHS are found to intersect at 6 different points; thus (18) admits 6 distinct solutions under this injection scenario, of which the second, fourth and sixth intersection points from the left denote dynamically stable solutions as explained previously. Fig. 8 shows the corresponding forced transient simulation. As before, the output waveform is found to show two (of three possible) distinct phase relationships with the turquoise waveform depicting $\overrightarrow{SYNC}(t)$. Momentary disturbances (depicted in magenta) shift the output waveforms from one lock state to the other, which are mutually separated by a third of one complete oscillation cycle as observed in the figure.

(a) Adlerized SHIL predicts marginal lock.
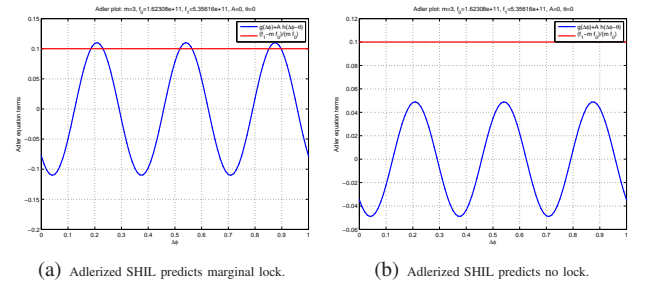

(b) Adlerized SHIL predicts no lock.

Fig. 9: Symmetric ring osc.: Adlerized SHIL equation predicting weak and no locking.

Fig. 9(a) shows the Adler plot case (b). The RHS and LHS waveforms only marginally intersect at 6 points with 3 dynamically stable solutions for injection locking as before. Intuitively, the possibility of a lock in the actual forced transient simulation is questionable, because of:

(1) the fact that an approximation was involved in the Adlerization process which ironed out the effect of the fast variations in $g(\theta(t))$. Incorporation of those variations would imply a fluctuation in the

required, along with a suppression of the 2nd harmonic component to prevent the probability of $m = 2$ SHIL. As noted previously, this can be easily achieved by reverting the P and N transistors in each inverter of the 3-stage ring oscillator to a symmetrized form; we chose $W_N = W_P = 0.3\mu$m. The effect of this change is readily noticeable in the natural oscillation waveforms of Fig. 7(a) which are symmetric about their mean voltage. This translates to the PPV waveforms in time and frequency domain as in Fig. 7(b) and Fig. 7(c) respectively; the suppression of the 2nd harmonic as compared to the 3rd is observed in the latter.

The predictions of the Adlerized SHIL equation (18) are tested for three cases:

(a) with sufficient amplitude or within a sufficiently small frequency deviation Δf to ensure a strong lock in the Adler plot (Fig. 7(d));

(b) with a critical amplitude or frequency deviation so that the Adler plot only predicts a marginal lock (Fig. 9(a));

(c) with a weak injection amplitude or sufficiently large frequency deviation so that the Adler plot clearly predicts no possibility of locking (Fig. 9(b)).
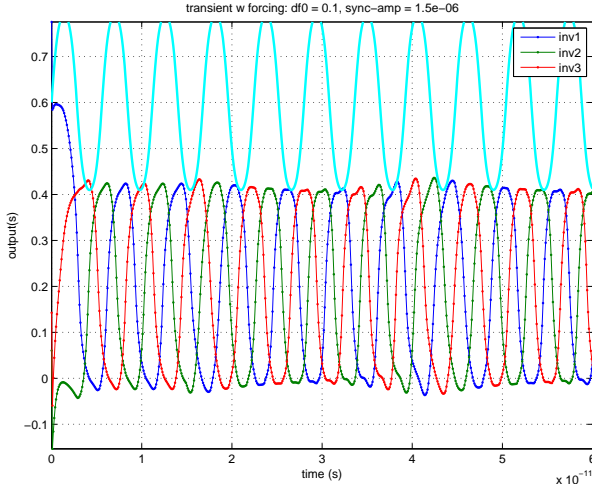
Fig. 10: Transient simulation of symmetric ring oscillator under marginal lock, showing beats.
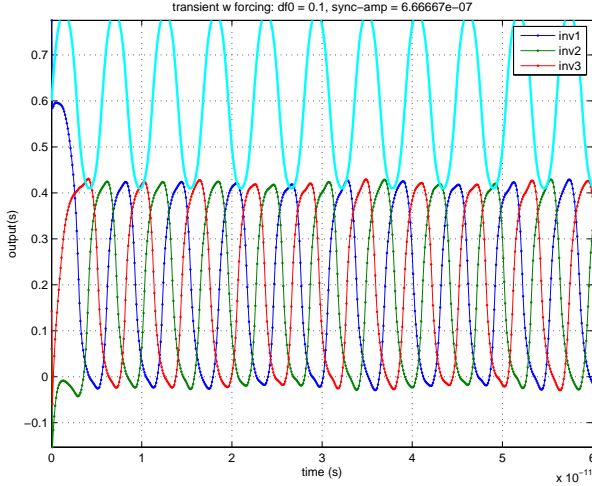

Fig. 11: Transient simulation of unlocked symmetric ring oscillator.

amplitude of the RHS (blue waveform) which in the present case can be sufficient to throw the oscillator out of lock;

(2) the fact that the separation between alternate solutions of Fig. 9(a) is highly skewed. This implies that when the oscillator is thrown out of lock as in (1) above, the solution would cross over the maxima of the blue waveform to migrate to the next stable solution point unidirectionally. However, as this point is also prone to the same variations as noted in (1), the solution would continue to migrate, essentially contributing an extra $\left(\frac{d\theta}{dt} \right)$ component. This translates to an additional frequency, characteristic of injection pulling rather than injection locking.

Fig. 10 shows the transient simulation for case (b). Close inspection of the output waveforms against the REF(t) waveform depicted in turquoise shows that the output has not phase-locked to the reference. Moreover, the output shows beat-like patterns, typically encountered in injection pulling scenarios. Between two such beat patterns the REF(t) waveform is seen to shift by a third of one complete oscillation cycle, indicative of the migration of the solution point of Fig. 9(a).

Finally, Fig. 9(b) shows the Adler plot for case (c). The LHS and RHS have no intersection, implying no solution for (18). This expectation is reflected in the forced transient simulation of Fig. 11. Inspection of the output waveforms against the turquoise REF(t) signal clearly shows no injection locking.

V. Conclusions

We have presented a powerful and general approach for analysing sub-harmonic injection locking (SHIL) in oscillators. The approach takes full account of the inherently nonlinear phase dynamics that underlie SHIL, yet arrives at a simple and intuitive equation that captures SHIL for any oscillator topology and any intended mode of sub-harmonic lock. The equation provides useful design insights for enhancing SHIL, and also provides precise information about the number, stability and robustness of sub-harmonic phase locks. We have demonstrated the new SHIL analysis technique using ring and LC oscillators as examples, and shown that its predictions are in excellent agreement with detailed SPICE-level simulations.

References

[1] R. Adler. A study of locking phenomena in oscillators. *Proc. IEEE*, 61:1380–1385, 1973. Reprinted from [11].

[2] B. Razavi. A study of injection pulling and locking in oscillators. In *IEEE CICC 2003*, pages 305–312, October 2003.

[3] Yayun Wan, Xiaolue Lai, and J. Roychowdhury. Understanding injection locking in negative-resistance LC oscillators intuitively using nonlinear feedback analysis. In *Proceedings of the IEEE Custom Integrated Circuits Conference*, pages 729–732, 18-21 Sept. 2005.

[4] P. Kinget, R. Melville, D. Long, and V. Gopinathan. An injection-locking scheme for precision quadrature generation. *IEEE Journal of Solid-State Circuits*, 37(7):845–851, July 2002.

[5] L. Goldberg, H.F. Taylor, J.F. Weller, and D.M. Bloom. Microwave signal generation with injection-locked laser diodes. *Electronics Letters*, 19(13):491–493, June 1983.

[6] H.R. Rategh, H. Samavati, and T.H. Lee. A CMOS frequency synthesizer with an injection-locked frequency divider for a 5-GHz wireless LAN receiver. *IEEE Journal of Solid-State Circuits*, 35(5):780–787, May 2000.

[7] S. Kudszus, M. Neumann, T. Berceli, and W.H. Haydl. Fully integrated 94-GHz subharmonic injection-locked PLL circuit. *IEEE Microwave and Guided Wave Letters*, 10(2):70–72, Feb 2000.

[8] Yuen Hui Chee, A.M. Niknejad, and J.M. Rabaey. An Ultra-Low-Power Injection Locked Transmitter for Wireless Sensor Networks. *IEEE Journal of Solid-State Circuits*, 41(8):1740–1748, Aug 2006.

[9] J.C. Leloup and A. Goldbeter. Toward a detailed computational model for the mammalian circadian clock. *Proc. National Academy of Sciences*, pages 7051–7056, June 2003.

[10] S. Agarwal and J. Roychowdhury. Efficient Multiscale Simulation of Circadian Rhythms Using Automated Phase Macromodelling Techniques. In *Proc. Pacific Symposium on Biocomputing*, volume 13, pages 402–413, January 2008.

[11] R. Adler. A study of locking phenomena in oscillators. *Proceedings of the I.R.E. and Waves and Electrons*, 34:351–357, June 1946. Reprinted as [1].

[12] S. Verma, H.R. Rategh, and T.H. Lee. A unified model for injection-locked frequency dividers. *IEEE Journal of Solid-State Circuits*, 38(6):1015–1027, Jun 2003.

[13] P. Bhansali and J. Roychowdhury. Gen-Adler: The generalized Adler's equation for injection locking analysis in oscillators. In *Proc. IEEE ASP-DAC*, pages 522–227, January 2009.

[14] X.Zhang, X.Zhou, B.Aliener, and A.S.Daryoush. A Study of Subharmonic Injection Locking for Local Oscillators. *IEEE Microwave and Guided Wave Letters*, 2(3):97–99, March 1992.

[15] A. Winfree. Biological Rhythms and the Behavior of Populations of Coupled Oscillators. *Theoretical Biology*, 16:15–42, 1967.

[16] A. Demir, A. Mehrotra, and J. Roychowdhury. Phase noise in oscillators: a unifying theory and numerical methods for characterization. *IEEE Trans. Ckts. Syst. – I: Fund. Th. Appl.*, 47:655–674, May 2000.

[17] A. Demir and J. Roychowdhury. A Reliable and Efficient Procedure for Oscillator PPV Computation, with Phase Noise Macromodelling Applications. *IEEE Trans. on Computer-Aided Design*, pages 188–197, February 2003.

[18] Jaijeet Roychowdhury. Numerical simulation and modelling of electronic and biochemical systems. *Foundations and Trends in Electronic Design Automation*, 3(2-3):97–303, December 2009.

[19] C. Gear. Simultaneous Numerical Solution of Differential-Algebraic Equations. *IEEE Trans. Circuit Theory*, 18(1):89–95, Jan 1971.

[20] X. Lai and J. Roychowdhury. Capturing injection locking via nonlinear phase domain macromodels. *IEEE Transactions on Microwave Theory and Techniques*, 52(9):2251–2261, September 2004.